An Interaction Potential to Study the Thermal Structure Evolution of a Thermoelectric Material: β-Cu_2Se

Sadanandam Namsani,[a] Bhasker Gahtori,[b] Sushil Auluck,[b] and Jayant K. Singh*[a]

An interaction potential model has been developed, for the first time, for β-Cu_2Se using the *ab initio* derived data. The structure and elastic constants of β-Cu_2Se using the derived force-field are within a few percent of DFT derived structure and elastic constants and reported experimental structure. The derived force-field also shows remarkable ability to reproduce temperature dependent behavior of the specific heat and thermal expansion coefficient. The thermal structure evolution of the β-Cu_2Se is studied by performing the molecular dynamic simulations using the derived force-field. The simulation results demonstrate that the Cu ions moves around the equilibrium lattice position within the temperature range of 500–800 K. However, at a temperature $>$ 800 K, the Cu ions starts diffusing within the material, while the Se ions remains in their lattice position. The evaluated thermodynamic properties such as free energy and excess entropy, show that the increased Cu–Se interaction with the temperature makes the system more thermodynamically stable. © 2017 Wiley Periodicals, Inc.

DOI: 10.1002/jcc.24865

Introduction

The solid state thermoelectric (TE) technology has gained significant attention due to its wide applications in waste heat recovery and thermal management applications.[1–3] Wide variety of alloys, bulk, and nanostructured TE materials, such as BiSbTe, β-Zn_4Sb_3, $CsBi_4Te_6$, PbTe, PbSe alloys, and bulk nanocomposite materials have been studied extensively by various researchers.[4–9] The choice of TE material depends on the range of operation temperature of applications. Thus, it is imperative to study the thermal structure evolution of TE materials.

One of the prominent TE materials Cu_2Se exists in two phases, a low temperature phase (α-Cu_2Se) and a high temperature phase (β-Cu_2Se). This material exhibits a phase transition, from a low temperature α-phase to a high temperature face-centered cubic β-phase, at 410 K.[10,11] Various studies have reported different structures for α-Cu_2Se,[12–16] and thus structure of the room temperature α-Cu_2Se is not clear. Unlike room temperature phase, β-Cu_2Se is shown to have a face centered cubic (fcc) structure for Se atoms with Cu atoms randomly distributed at different sites.[10,11,14,17,18] The liquid like behavior of Cu ion with rigid fcc cubic lattice Se atoms of β-Cu_2Se is shown to be a very good TE material with a TE figure of merit, ZT, of 1.5 at 1000 K.[10] This ZT value is considerably higher than the commercially available TE materials, which have ZT $\sim$ 1.[19] This shows β-Cu_2Se is a highly promising material for various thermal management and electronic applications. Despite clear structure with respect to the Se atoms, β-Cu_2Se shows significant anomalies in thermophysical and structural properties with change in temperature. The anomalous behavior includes decrease in heat capacity of the system to the theoretical limit of liquids ($\sim 2k_B$, where k_B is Boltzmann constant),[10,20] a large coefficient of thermal expansion (CTE), 10.7×10^{-5} K^{-1}, at 800 K.[10] This complicated material physics and temperature dependency of the properties of β-Cu_2Se make the study of this material challenging theoretically and experimentally. Despite the challenges involved in studying this material, several authors reported the structural and thermophysical properties using experiments.[10,11,20] However, the anomalous structural and thermophysical properties associated with the thermal structure evolution and related physics are not clearly understood. The atomistic simulations are very useful in this case to explain the related physics of the system. Kim et al.[20] used *ab initio* molecular dynamics (MD) simulations to study the structural evolution of β-Cu_2Se. To predict macroscopic properties of a system using MD simulations, one needs to consider system of large size. The *ab initio* simulations are computationally expensive and performing simulations of large system size is difficult. The MD simulations using molecular mechanics potential model are useful to perform simulations of such a large system size. However, to reproduce the properties of the system accurately using molecular mechanics MD simulations, the potential model should be accurate enough. So far, no interaction potential is reported for β-Cu_2Se, which is necessary to study the structural and transport properties using MD simulations.

In this article, we have reported a potential model for β-Cu_2Se, which reproduces the structure and thermophysical properties accurately. The temperature dependency of the CTE

[a] S. Namsani, J. K. Singh
Department of chemical engineering, Indian Institute of technology Kanpur, Kanpur 208016, India
E-mail: jayantks@iitk.ac.in
[b] B. Gahtori, S. Auluck
Materials Physics and Engineering Division, CSIR-National Physical Laboratory, CSIR-Network of Institutes for Solar Energy, Dr. K. S. Krishnan Road, New Delhi 110012, India
Contract grant sponsor: Department of Science and Technology (DST), India

Table 1. β-Cu_2Se structure crystallographic data from experiments.[10,11]

Lattice constant (Å)	5.864		
Space group	*F*m-3m		
	Wyckoff positions		
Atom	Position	(*x*, *y*, *z*)	Charge
Se	4a	(0,0,0)	2-
Cu	8c	(1/4, 1/4, 1/4)	1+
Coulomb's constant (*C*)		332.07 kcal/mole	

and heat capacity are well reproduced using the derived force-field. Furthermore, to attain an understanding of the change in the properties associated with the change in the thermal structure of β-Cu_2Se, we have performed MD simulations in the temperature range of 500–1000 K. The average structure of the system is analyzed by computing the radial distribution function (RDF) of the Cu—Cu, Cu—Se, and Se—Se pairs. Finally, the thermodynamic properties, free energy and excess entropy, are evaluated to understand the mechanism responsible for anomalies in the structural and thermophysical properties of β-Cu_2Se.

Model and Methodology

Model for β-Cu_2Se interatomic potential

In this work, we have developed the interaction potential model for β-Cu_2Se. To model the potential parameters for β-Cu_2Se, we use a two-body potential model to account for the interactions between the pair of atoms *i* and *j*. The potential form also consists of a columbic term, which accounts for the long-range electrostatic interactions. The two-body potential we chose is the Morse potential, which is shown to be a good approximation to predict vibrational properties of materials. Similar type of potential was also used successfully to model TE materials like, Bi_2Te_3,[21] Mg_2SiSn,[22] and MoS_2.[23] The potential model used in this study is expressed in the form of eq. (1), which is shown below.

$$E_{ij}=D\left[\left\{\left(1-\exp\left(-a(r_{ij}-r_0)\right)\right\}^2-1\right]+\frac{Cq_iq_j}{r_{ij}} \quad (1)$$

where, E_{ij}, is the interaction energy of a pair of atoms, *i* and *j*, (which are atomic indexes and is either a Cu or a Se atom). *D*, *a*, r_0, and *C* are the dissociation energy, bond elasticity (controls the width of the potential), equilibrium bond length, and coulomb's constant, respectively. model parameters. Here, q_i and q_j are the charges of atoms considered in this model.

Method for evaluation of potential parameters

The potential model for the Cu_2Se system is derived by fitting potential parameters to various reference structures and corresponding total energies obtained using DFT calculations. To derive the potential parameters, we optimize the model parameters until the calculated and the reference energies are as close as possible, which is performed by minimizing the following function using method of least square fitting:

$$F=\sum_{i=1}^{N_{obs}} w_i\left(f_i^{obs}-f_i^{calc}\right)^2, \quad (2)$$

where N_{obs} is the number of observables, *F* is the sum of squares, f_i^{calc} and f_i^{obs} are the calculated and the observed values, and w_i is a weighting factor. The procedure to estimate the potential parameter is performed using the GULP program.[24,25]

Observables for β-Cu_2Se potential fitting. The observables used in the fitting procedure are the total energies of the β-Cu_2Se obtained by varying the lattice parameter around its equilibrium value, while preserving the bulk symmetry of the structure. To generate the data, we have performed DFT calculations using a unit cell containing 12 atoms. The FCC unit cell constructed using the crystallographic data (see Table 1), with Cu distributions at (0.25, 0.25, 0.25) and Se distributions at (0.0, 0.0, 0.0), is shown in Figure 1.

The technical details of the DFT calculations are given in the next section. Unit cells of different volume are generated by varying the lattice parameter around the experimental unit cell parameter. The equilibrium lattice parameter used to generate the structures is 5.864 Å. We have calculated the total energies for lattice constants varying from 5.104 to 6.604 Å.

DFT calculations. We used DFT within the full potential linear augmented plane wave (*FPLAPW+lo*) method in a scalar relativistic version as embodied in the *WIEN2k* code.[26] The exchange-correlation (*XC*) potential is solved using the generalized gradient approximation (GGA), which is based on exchange-correlation energy optimization. We have used the exchange correlation potential given by Perdew, Burke and Ernzerhof (PBE).[27] It is well-known that in calculating the self-consistent band structure within DFT, the GGA approximation

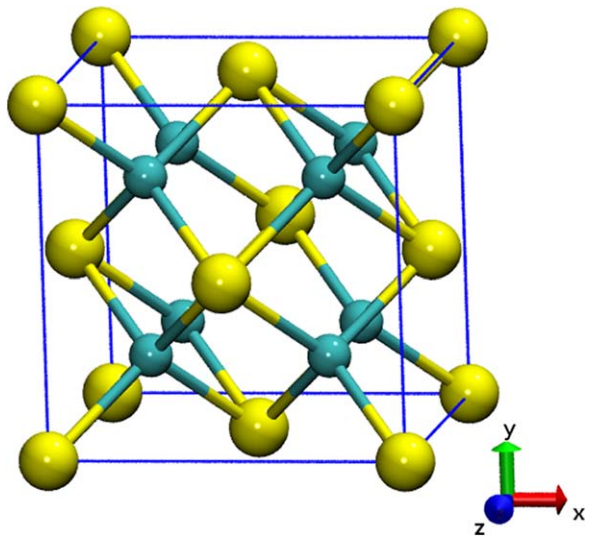

Figure 1. The FCC unit cell of β-Cu_2Se; yellow (Se) and cyan (Cu). [Color figure can be viewed at wileyonlinelibrary.com]

underestimates the energy band gap by around 10–30%. This is mainly due to the fact that GGA has a simple form that is not sufficiently flexible to accurately reproduce both the exchange–correlation energy and its charge derivative. As a result, we do not get an energy gap for Cu_2Se in the fluorite structure. The Kohn–Sham equations are solved using a basis of linear *APW's*. The convergence of the basis set is controlled by a cut off parameter RK_m, which is defined as $RK_m = R_{mt} \times K_{max}$. The parameters R_{mt} and K_{max} are the smallest of all atomic sphere radii and the plane wave cut-off, respectively. We have taken $RK_m = 7.0$. The potential and charge density in the muffin-tin (*MT*) spheres are expanded in spherical harmonics with $l_{max} = 10$ and/or non-spherical components up to $l_{max} = 4$. In the interstitial region, the potential and the charge density are represented by Fourier series. Self-consistency is obtained using 165 $\vec{k}$ points in the irreducible Brillouin zone (*IBZ*). The self-consistent calculations are converged as the total energy of the system is stable within 0.00001 Ry.

MD simulations. All MD simulations, using the derived force-field, are performed using the LAMMPS code.[28] To study the thermal structure evolution, we have considered a super cell of β-Cu_2Se system with a simulation box length of 35.36 Å. The MD simulations are performed at different temperatures from 500 to 1000 K. First, the simulation system is equilibrated for 5 ns at the desired temperature and 1 bar pressure using the isothermal and isobaric ensemble (NPT) simulations. This allows the system to change the simulation box size according to the thermal expansion coefficient at that temperature. After 2 ns of NPT simulations, we have not seen any change in simulation box size with simulation time. The equilibrated structure obtained from the NPT simulations (considered after 5 ns run) is further subjected to the isothermal and constant volume ensemble (NVT) simulations for 2 ns to get the final equilibrated structure pertaining to the desired temperature. Furthermore, the equilibrated structure obtained from NVT simulations is simulated using micro canonical ensemble (NVE) for 2 ns. Finally, the production runs are performed for 1 ns under NVE ensemble to get the desired structural properties. An interaction cut-off of 12 Å is used to account the long-range electrostatic interactions within the system. These electrostatic interactions are taken into account using method of Ewald summation as implemented in LAMMPS code. Standard periodic boundary conditions are used in all three directions. To perform all MD simulations in different ensembles aforementioned, we have used a time step of 1 fs.

Lattice dynamics simulations. To evaluate the crystal properties like, elastic constants, different modulus, CTE, and phonon-based heat capacity at constant volume, we have used the lattice dynamics code, GULP.[24,25] The elastic constants are defined as the second derivative of the energy density with respect to strain as shown in the equation below.

$$C_{ij} = \frac{1}{V}\left(\frac{\partial^2 u}{\partial \varepsilon_i \partial \varepsilon_j}\right) \tag{3}$$

Here, C_{ij} are elastic constants, u is the energy, and ε is the strain. As minimization of free energy results in the volume

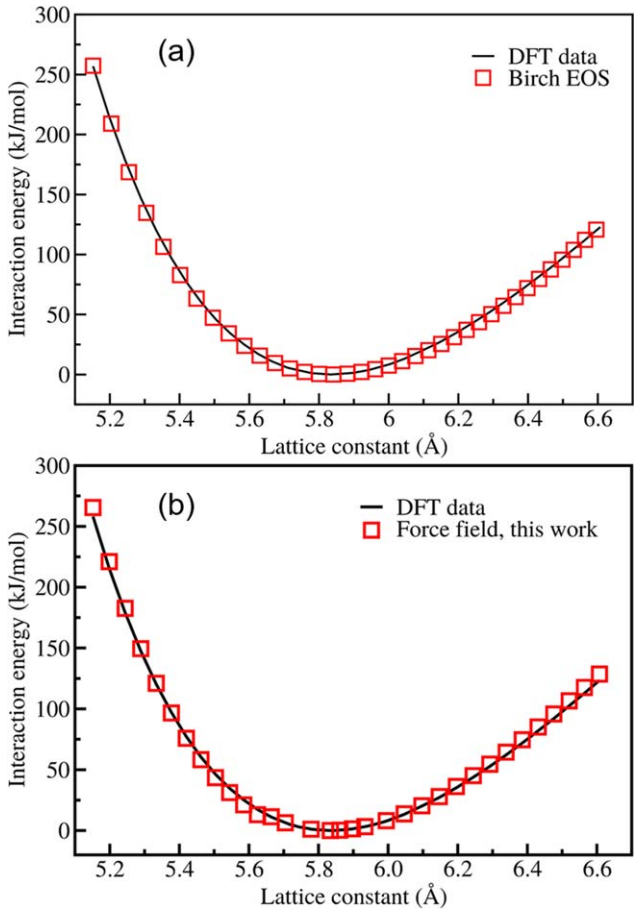

Figure 2. a) Energy-volume data generated using DFT for β-Cu_2Se structure. The red square symbols in curve represent the fit to the Birch-EOS. b) A comparison of energy-volume data obtained from DFT (black line) and the new empirical force-field (red squares). [Color figure can be viewed at wileyonlinelibrary.com]

expansion of the material,[29] we have used the free energy minimization method implemented in GULP program to calculate the thermal expansion coefficient. The zero internal stress approximation is used to perform these calculations. This is shown to be a good approximation to predict the CTE for the silica polymorphs.[30] The thermal expansion coefficient that is reported in this study is the linear thermal expansion coefficient, which is defined as $(\Delta a/a)/\Delta T$. Here, a is the lattice parameter and T is the temperature.

In the case of solids, usually the translational and rotational contributions can be neglected. Moreover, the electronic contribution is directly calculated via interatomic force-field. This simplifies the challenge of calculating the total energy to measurement of vibrational properties. Thus, in this work, the heat capacity is calculated using vibrational partition function, Z_{vib}. The equation form of the partition function is shown below.

$$Z_{vib} = \sum_{k\text{-points}} w_k \sum_{\text{allmodes}} \left(1 - \exp\left(-\frac{h\nu}{k_B T}\right)\right)^{-1} \tag{4}$$

where h, ν, k_B, T, and w are Plank's constant, frequency, Boltzmann constant, temperature, and weighing functions. Using the vibrational partition function, one can readily calculate the

Table 2. Comparison of the DFT computed unit cell parameters and bulk modulus for β-Cu_2Se with experimental and literature data.

Parameter	Present work	Experimental data	Literature DFT data
Lattice constant (Å)	5.838	5.864[a][b]	5.844,[c] 5.833[c]
Bulk modulus (GPa)	80.06		81.00,[c] 82.00[c]

Liu et al.[10] Yu et al.[11] Råsander et al.[32]

heat capacity at constant volume, C_v, using the below equation.

$$C_v = RT\left(2\left(\frac{\partial \ln Z_{vib}}{\partial T}\right) + T\left(\frac{\partial^2 \ln Z_{vib}}{\partial T^2}\right)\right) \quad (5)$$

where R is the gas constant and T is the temperature. The C_v values obtained using the above method agree reasonably well with the energy fluctuations method particularly at lower temperatures. Nevertheless, both the methods yield the same behavior of C_v against temperature.

Results and Discussions

Structural properties of β-Cu_2Se

Initially, to assess the quality of the DFT data, the computed energy-volume data for the β-Cu_2Se is fitted to the Birch-Murnaghan equation of state[31] (Birch-EOS) to get the equilibrium lattice constant and bulk modulus. The DFT data and the fit of Birch-EOS to the DFT data are shown in Figure 2a.

The bulk modulus and the equilibrium lattice constant obtained using Birch-EOS fitted to the DFT data are 5.838 Å and 80.06 GPa, respectively. The comparison of the data obtained from this work with that of the literature is shown in Table 2.

The lattice constant obtained from the fit is in very good agreement with the experimental lattice constant[10,11] as well as with the reported DFT-based lattice constant.[32] The bulk modulus value is also in very good agreement with the DFT data reported in literature.[32] The error associated with the prediction of the bulk modulus is 1.16%, when compared with the value reported by Råsander et al.[32] using DFT calculations. Clearly, this shows that the energy-volume data generated using DFT calculations is accurate enough to develop an interatomic potential model for Cu_2Se. To this end, we utilized the DFT-based energy-volume data of the Cu_2Se structure to obtain the force-field parameters using the least square fitting procedure given in model and methodology section. The derived potential parameters for Cu_2Se are tabulated in Table 3.

Table 3. β-Cu_2Se potential parameters obtained using the DFT-based energy-volume data.

Morse potential	D (eV)	a (1/Å)	r_0 (Å)	Cut-off (Å)
Cu-Cu	0.1517	1.3917	3.00	3.5
Cu-Se	0.4370	3.0341	2.44	3.5
Se-Se	0.9745	0.6057	4.68	4.5

Table 4. Comparison of structural and elastic properties calculated using the derived force-field and DFT.

Parameter	This work (force-field)	This work DFT data
Lattice constant (a, Å)	5.838	5.838 (5.864[a][b])
Bulk Modulus (GPa)	89.43	89.276
C_{11} (GPa)	121.28	121.298
C_{12} (GPa)	73.50	73.419
C_{44} (GPa)	73.50	74.101

Liu et al.[10] Yu et al.[11] These results are also compared with experiments (shown in brackets) and other theoretical work. C_{11}, C_{12}, and C_{44} are elastic constants.

To assess the quality of the new force-field, first we have calculated the structural parameters of Cu_2Se, using the new force-field, and are summarized in Table 4. We have also performed DFT calculations to calculate the elastic constants and bulk modulus and are given in Table 4 for comparison. It should be noted that the Cu_2Se structure experimental data are very scarce. Nevertheless, we have compared the simulation results with the available experimental and theoretical data. The new force-field underestimates the cell parameter by only 0.44% with respect to the experimental data of Liu et al.[10] and Yu et al.[11] This value is also in good agreement with earlier DFT calculation of Råsander et al.[32] using PBE and PBE0 methods. The bulk modulus value obtained from the generated force-field is 89.43 GPa. The calculated bulk modulus value is in very good agreement with the value obtained through DFT calculations in this work. The elastic constants (C_{11}, C_{12}, and C_{44}) obtained using the generated force-field are in good agreement with the values obtained using DFT calculations. The error associated with prediction of C_{11} and C_{12} is less than 0.2%, when compared with the DFT values. The C_{44} is underestimated by 0.8% compared to the obtained DFT value.

Furthermore, to evaluate the potential parameters, we have also computed the energy-volume data using the generated force-field. The energy-volume data obtained using our force-field is in very good agreement with that obtained from DFT computations, which is clearly evident from Figure 2b.

Temperature dependent properties evaluation

Thermophysical properties. The β-Cu_2Se is a TE material, which exhibits highly temperature sensitive thermophysical properties. Hence, it is very crucial for the potential to reproduce the temperature dependent properties of the material accurately. To this end, we have computed the CTE and heat capacity (C_v) at different temperatures using free energy minimization of the structure. The behavior of the heat capacity with the temperature is shown in Figure 3a. The C_v values computed within the temperature range of 500–1000 K are in very good agreement with the values reported experimentally by Liu et al.[10] and Kim et al.[20] The C_v value decreases from the theoretical limit of solid ($3Nk_B$) to the liquid ($\sim 2Nk_B$) with the increase in temperature. We observe sudden decrease in the C_v at a temperature of 800 K, and this decreasing trend is

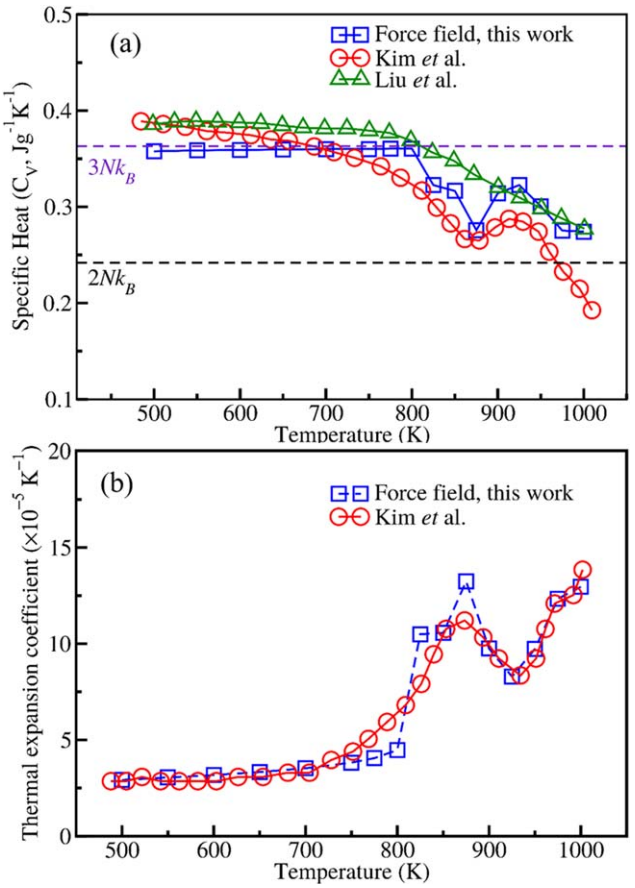

Figure 3. a) Comparison of heat capacity data obtained using the generated force-field with the experimental data. b) Comparison of CTE obtained using the generated force-field with the experimental data. [Color figure can be viewed at wileyonlinelibrary.com]

continued up to a temperature of 850 K. Subsequent increase in temperature, that ias, beyond 850 K increase in the C_v value until 925 K is seen. At temperatures higher than 925 K, we observe change in the C_v behavior, which again decreases continuously up to a temperature of 1000 K. It is evident that the decreasing trend in C_v is not continuous with the temperature. Between 875 and 925 K, there is an increase in heat capacity, and this type of behavior within the aforementioned temperature range is in agreement with the Kim et al.[20] reported experimental data.

Figure 3b shows the computed CTE at different temperatures along with experimental data.[20] The CTE increases monotonously from 2.5 $\times$ 10^{-5} K^{-1} at 500 K to 5.0 $\times$ 10^{-5} K^{-1} at 800 K. However, CTE behavior is non-monotonous at temperatures higher than 800 K. At a temperature slightly higher than 800 K, we observe an enormous jump in CTE value to $\sim$10.5 $\times$ 10^{-5} K^{-1}. This value is consistent with the reported value 10.7 $\times$ 10^{-5} K^{-1} at 800 K.[10] The computed CTE at the considered temperatures are in very good agreement with the Kim et al.[20] reported experimental data. This sudden expansion in the material at 800 K may be attributed to the initiation of Cu ion diffusion within the material. This sudden expansion with the Cu ion diffusion may be the reason for the decrease in heat capacity with the temperature.

Mechanical properties. Figure 4a presents the computed elastic constants C_{11}, C_{12}, and C_{44} at different temperatures. These elastic constants reflect the strength of the interatomic forces in the solid. The material that is considered here is a cubic material and stability criteria concern the following equations.[33] The cubic structure is stable if it satisfies the equations given below:

$$C_{11} > 0;\ C_{12} > 0;$$
$$C_{11} - C_{12} > 0;\ C_{44} > 0.$$

With the elastic constants shown in Figure 4a, all the computed elastic constants satisfy the aforementioned equations for the considered temperature range. This shows the structure is mechanically stable structure. With the increase in temperature, we found decreasing trend for C_{11}, and C_{12}. This type of behavior is also seen in other TE material like SnTe.[34] This is an indicative of the loss of material rigidity with the temperature. In case of C_{44}, we found decreasing trend on increasing the temperature from 500 to 800 K. At a temperature slightly higher than 800 K, we observe a jump in the C_{44} value, and after that the value decreases up to 875 K. Between 875 and 925 again, we found increase in C_{44} value. The behavior of C_{44} again changes at the temperature range 925–1000 K, where it

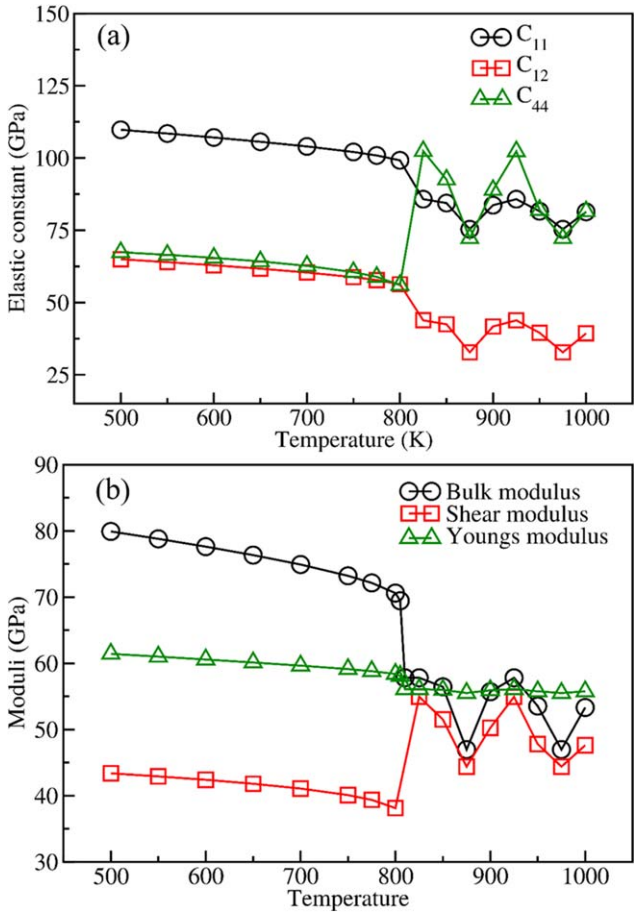

Figure 4. a) Change in elastic constants with temperature. b) Change in bulk, shear, and Young's modulus with the temperature. [Color figure can be viewed at wileyonlinelibrary.com]

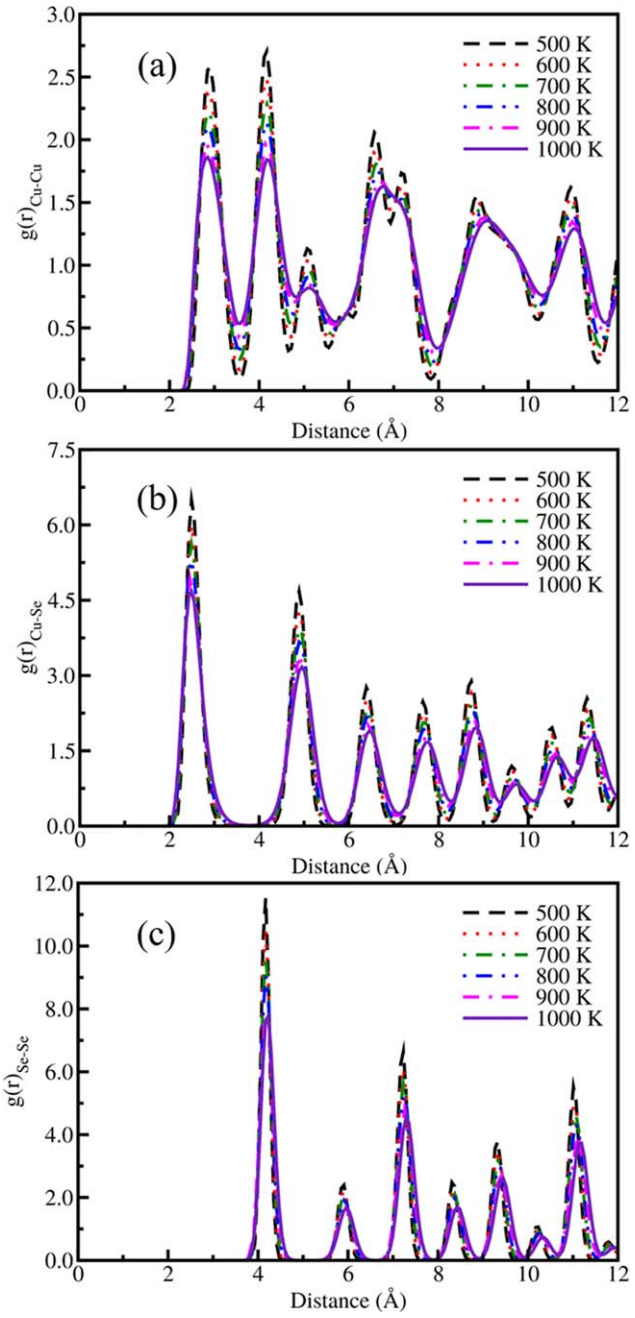

Figure 5. The RDF at different temperatures for a) Cu—Cu, b) Cu—Se, and c) Se—Se pairs. [Color figure can be viewed at wileyonlinelibrary.com]

is found to continuously decrease. The sudden increase in C_{44} at 800 K may be because of the sudden thermal expansion that we have observed in the system. From 825 to 925 K, the decrease and increase in the C_{44} value may be attributed to the change in diffusion and atomic positional rearrangement of the Cu ion with the temperature.

Figure 4b shows the bulk modulus, shear modulus and Young's modulus computed at different temperatures. The moduli that are aforementioned are derived from the computed elastic constants C_{11}, C_{12}, and C_{44}. So the change in elastic constants with temperature is also reflected in the computed moduli. The bulk modulus and Young's modulus decrease with increasing temperature. As shear modulus is computed using the C_{44},[35,36] its behavior is analogues to that of C_{44}. The shear modulus is found decrease with the increase in temperature up to 800 K. There is a sudden increase in the Shear's modulus at 800 K similar to that seen for C_{44}. The behavior beyond 800 K is also akin to that seen for C_{44}.

Structural properties. To understand the structural evolution with the temperature, we have computed the RDF using the MD simulations, which is useful in describing the average structure of the system. The RDF also allows one to connect the structure with the thermodynamic and transport properties.[37] The computed RDFs for Cu—Cu, Cu—Se, and Se—Se pairs at different temperatures are shown in Figures 5a–5c, respectively.

For a perfect crystal structure, the RDF for any pair of atoms is represented as a series of sharp peaks at distinguished positions. In this work, the Cu—Cu RDF is expected to be a series of sharp peaks at different positions of Cu atoms. However, the RDFs obtained at different temperatures show broad peak with a wave like nature. This behavior suggests a thermally disordered Cu ion motion within the system. The peaks in the RDF profile are more broadened in nature and reduced in height with increasing temperature. The first peak position in RDF represents the average distance between the two nearest neighbors. The first peak position of the Cu—Cu RDF at different temperatures, that is, 500, 600, 700, 800, 900, and 100 K are at 2.94, 2.82, 2.82, 2.82, 2.82, and 2.80 Å, respectively. This represents the average Cu—Cu bond distance. The obtained average Cu—Cu bond distance at 500 K is 2.94 Å, which is expected bond distance in an ideal symmetry structure of β-Cu_2Se.[20] For temperatures greater than 500 K, the Cu—Cu bond distance is less than the 2.94 Å. This shows the tendency of the Cu ions to occupy multiple interstitial sites within the material. The peak height at this position is found to decrease with increasing temperature. This indicates the decrease in the local density of Cu ions with respect to the uncorrelated bulk density about a fixed Cu ion. This decrease in peak height with the temperature is also observed for other peaks in the RDF profiles. Moreover, we have also observed the fading of peak split in RDF profile with the increase in temperature at 5.0 and 7.0 Å. At temperatures 900 and 1000 K, the split in the peak of RDF at 7.0 Å completely disappear and a single broad peak is observed in that position. This nature suggests relaxation of the atomic arrangement at those respective positions.

Furthermore, to see the structural arrangement of Se atoms with respect to Cu atoms, we have computed the RDF for Cu—Se at different temperatures and the obtained RDF profiles are shown in Figure 5b. The RDF profiles show series of peaks up to a distance of 7 Å. After 7 Å, we have seen broad peaks with wave nature. The three series of sharp peaks within 7 Å indicates the Se atoms that form stable coordination shells around a fixed Cu atom. After 7 Å, the atoms in coordination shells are not that rigid at their position, as seen in the RDF profiles for the distance less than 7 Å, which results in broadened peaks and wave nature in RDF. The peaks in the RDF profile are slightly broadened in nature and reduced in height

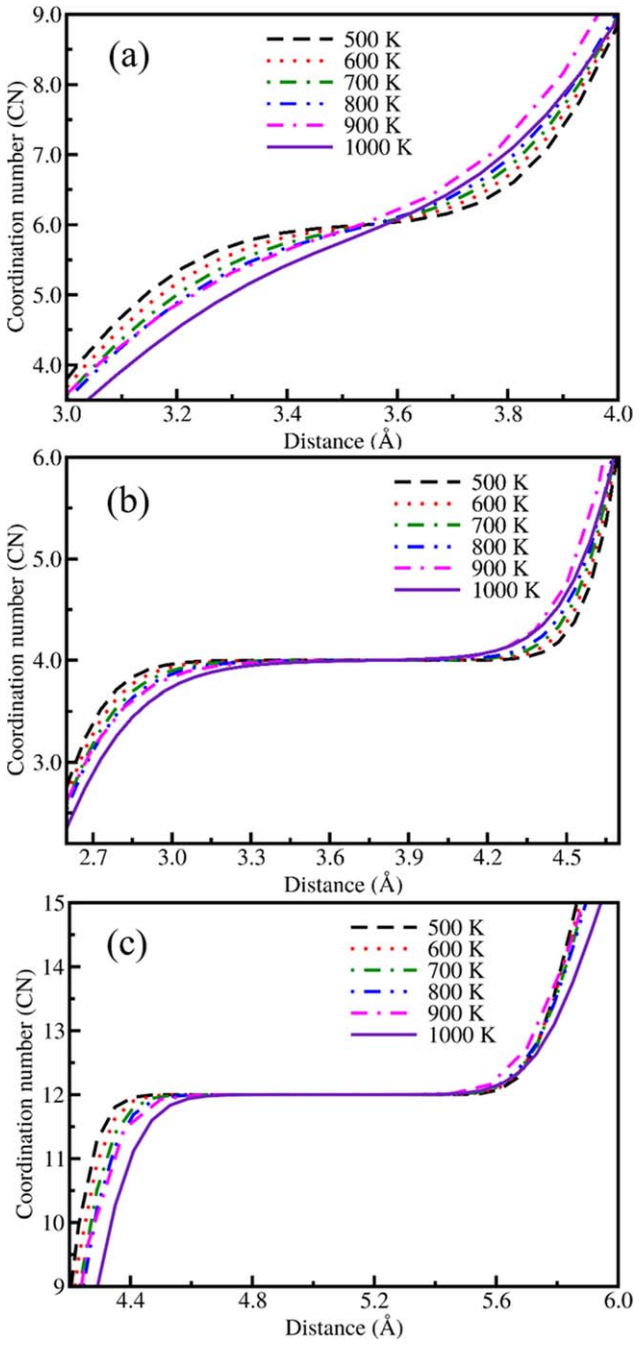

Figure 6. Coordination number for a) Cu—Cu, b) Cu—Se, and c) Se—Se at different temperatures. [Color figure can be viewed at wileyonlinelibrary.com]

with the increase in temperature This broadening indicates the presence of increased disordered atoms with increasing temperature. This is mainly because of the anharmonic thermal vibrations of the atoms. This behavior is similar to that seen for the case of Bi_2Te_3 TE material.[38] For all the temperatures, the position of the first peak is observed at 2.46 Å. Furthermore, the height of the first peak is found to be decreasing with the temperature, which is also seen in case of Cu—Cu RDF.

In addition, we have also computed the RDF for Se—Se pair at different temperatures and the obtained RDF data is shown in Figure 5c. This Se—Se RDF displays a series of peak at all the considered temperature. The peak positions are same, and peak heights are almost constant for the considered temperature range. This indicates the stable Se atom coordination around a fixed Se atom, which is the behavior typically seen in the crystal structures. Thus, it shows a strong tendency of Se atoms to remain in their rigid framework to maintain the crystal structure.

Furthermore, we have computed the coordination number (CN), the number of atoms around the selected atom type, in the first coordinate shell by integrating the RDF. The obtained CN profiles for Cu—Cu, Cu—Se, and Se—Se are shown in Figures 6a–6c, respectively.

The Figure 6a shows the CN of Cu atoms around a fixed Cu atom in the first coordination shell. A stable CN of 6 is observed for the temperature of 500 K (flat region in CN profile). After 500 K, we observe fading of stable coordination with the temperature, which indicates the free movement of the atoms. At 1000 K, there is no stable coordination of atoms in the system. The Cu atoms movement without a stable CN indicates liquid like behavior, which is consistent with the qualitative understanding obtained using the experiments.[10,11] In case of Cu and Se, a stable CN of 4 is observed at 500 K (see Fig. 6b). This CN is observed within the distance from 3.0 to 4.2 Å. With the increase in temperature the CN = 4 does not change, but the radius of the first coordination shell decreases. At 1000 K, we observe CN = 4 within the distance from 3.2 to 4.0 Å. This indicates the unstable coordination at temperatures more than 600 K. For Se—Se, we observe a stable CN of 12 for all the temperatures considered in this study (see Fig. 6c). This confirms rigid movement of Se atoms around their respective lattice positions. Thus, it is clear that within the system the Cu atoms move freely, while the Se atoms remain in their respective lattice positions at higher temperatures.

The RDF and CN analysis show the liquid like behavior for Cu atoms with the increase in temperature. This behavior can also be clearly shown by tracking the atomic trajectories of the atoms in the system. To generate these atomic trajectories, we have collected the unwrapped coordinates of atoms in a regular time interval of 1 ps during the NVE simulations. The trajectories of atoms for 3 ns simulations are shown in Figure 7. The trajectory of all atoms in the system is shown for 500 K simulations. For higher temperatures, 600–1000 K, zoomed in-view of a small segment of the system is shown for clear understanding.

For the temperature range of 500–700 K, the atomic trajectories show that the Cu atoms are thermally vibrating around their lattice position while the Se atoms almost remain rigid in their lattice positions. The Se atoms maintain the framework of the crystal. The structure viewed toward (100) plane, *XY*-plane, looks like Se and Cu atomic layers are alternatively stacked within the simulation box. The obtained atomic trajectory at 800 K displays increased movement of Cu atoms and movement of Cu atoms toward the Se atomic sites. Further increase in temperature to 900 K the Cu atoms diffuse toward the interstitial positions of Se atomic layers and Cu atomic layers. At 1000 K, the obtained atomic trajectory displays the diffusion of Cu atoms, accessing the interstitial positions of Se atomic layers as well as nearby Cu atomic sites. This type of

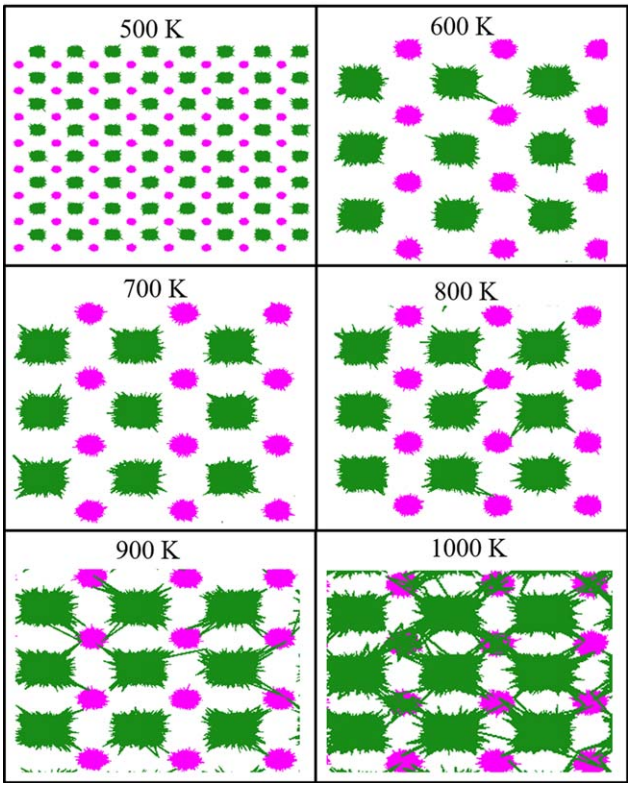

Figure 7. The atomic trajectories, unwrapped coordinates, of atoms in *XY*-plane at different temperatures. The Cu and Se atom trajectories are shown in green and pink color, respectively. [Color figure can be viewed at wileyonlinelibrary.com]

liquid like behavior may be the reason for the decrease in heat capacity of β-Cu_2Se to the theoretical limit of liquids.

Thermodynamic properties. The RDF and atomic trajectories show that the Cu atoms diffuse within the material to access the interstitial positions of Se atomic layers and other nearby Cu atomic positions. To understand the interaction behavior of atomic pairs, we have computed the potential of mean force (PMF) for the Cu—Cu and Cu—Se pairs. The PMF analysis has earlier been used by Shoko et al.[39] to understand the diffusion behavior of K in Al-doped defect pyrochlore tungstate, which is a TE material. In this work, the PMF profiles are evaluated, using the RDF data, as $\mathrm{PMF}(r) = -k_B T \ln(g(r))$. The PMF profiles obtained from the Cu—Cu and Cu—Se RDF data are shown in Figures 8a and 8b,, respectively.

The PMF profiles obtained for Cu—Cu pair for all the considered temperatures show three energy barriers with decreasing barrier height within a distance of 6 Å (see Fig. 8a). These energy barriers are located at 3.54, 4.74, and 5.7 Å, respectively. There are also three energy minima in the PMF profile. The three energy minima are located at 2.94, 4.14, and 5.25 Å, respectively. The first minima in the PMF profile (at 2.9 Å) is known as the first contact minima, which shows the free energy change associated with the aggregation of the corresponding atoms. This PMF value at this minimum is also referred as the free energy of aggregation (ΔG).[40] This position of first contact minima also refers to the equilibrium bond distance between the corresponding atoms. The PMF value for the first minima at 500, 600, 700, 800, 900, and 1000 K are −3.89, −4.12, −4.55, −4.85, −5.02, and −5.12 kJ/mol, respectively. This shows the increase in temperature favors the Cu atoms to stay at the first minima. The decrease in free energy is ∼29% at 1000 K with respect to the 500 K. The second minima (at 4.14 Å) corresponds to the Se layer separated contact minima for the Cu atoms. The PMF value at the second minima at 500, 600, 700, 800, 900, and 1000 K are −4.17, −4.39, −4.78, −4.97, −5.04, and −5.07 kJ/mol, respectively. This shows that the PMF values at first minima are higher than the values at second minima, which displays the high probability for the atom to stay at second minima position. The energy barrier between the first and second minima (at 3.54 Å) corresponds to the barrier for the Cu atoms to diffuse from one Cu layer to the other Cu layer separated by a Se atom layer. The energy barriers at 3.54 Å for 500, 600, 700, 800, 900, and 1000 K are 13.93, 12.40, 12.40, 11.98, 11.25, and 10.28 kJ/mol, respectively. The obtained energy barrier for Cu atoms diffusion at 500 K (13.93 kJ/mol) is in reasonable agreement with the reported average activation energy, 22.19 ± 4.82 kJ/mol, for Cu_2Se system in the temperature range of 373–473 K. This value is also in good agreement with the reported activation energy (13.51 kJ/mol) for Cu atoms diffusion in Al/Cu_2Se/Pt

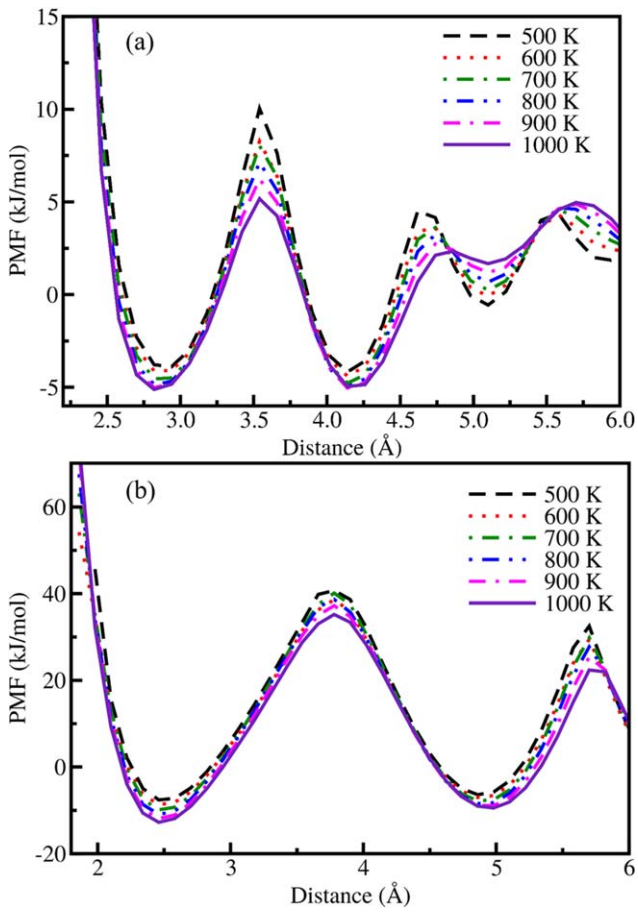

Figure 8. The PMF calculated at different temperatures using a) Cu—Cu and b) Cu—Se RDF data. [Color figure can be viewed at wileyonlinelibrary.com]

system in the temperature range of 395–408 K. The obtained energy barriers clearly show reduction in the barrier height with increasing temperature. The reduction in the energy barrier for 1000 K with respect to the 500 K energy barrier is ~26%. This shows that the increase in temperature favor the diffusion of Cu atoms from the first coordination shell. The second and third energy barriers are less than the first energy barrier observed at 3.54 Å. This indicates that once the Cu atoms diffuse to the second Cu layer, further diffusion of Cu atoms requires much less energy.

It is noted that the computed PMF profiles for the Cu—Se pair show a multiple minima and maxima. The first two minima indicate that the Se atoms are in the first two coordination shells around Cu atom. The two minima in the PMF located at 2.46 and 4.86 Å. The PMF values at the first contact minima (at 2.46 Å) for the 500, 600, 700, 800, 900, and 1000 K are −7.59, −8.69, −9.87, −10.93, −11.89, and −12.76 kJ/mol, respectively. The decrease in PMF value at the contact minima clearly suggests that the increase in temperature favors the aggregation of Cu and Se atoms. The PMF values at the second minima (at 4.86 Å) for the 500, 600, 700, 800, 900, and 1000 K are −6.38, −7.02, −7.82, −8.42, −8.94, and −9.45 kJ/mol, respectively. This indicates that minimum becomes deeper with increasing temperature, which shows the increased interaction of Cu and Se atoms with the temperature. The first energy barrier, in between the first and second minima, for the 500, 600, 700, 800, 900, and 1000 K is 48.32, 47.32, 50.0, 49.62, 49.12, and 47.96 kJ/mol, respectively. This clearly shows that with the increase in temperature from 500 to 600 K reduces the energy barrier. Further increase in temperature to 700 K increases the energy barrier. At 800 and 900 K, the energy barrier almost equal to the barrier energy at 700 K. At 1000 K, we observe 4% decrease in barrier height when compared to the energy barrier at 700 K. Thus, it is clear that increase in temperature to from 600 to 1000 K favors Cu–Se interactions.

The free energy of aggregation (PMF value at the first minima) for both Cu—Cu and Cu—Se decreases with the increase in the temperature from 500 to 1000 K (see Fig. 9a). This indicates the increase in temperature increases the driving force for the aggregation of both the pairs. For the considered temperature range, the free energy of aggregation for Cu—Se pair is more (more negative) compared to Cu—Cu pair, which suggests increased affinity for Cu—Se aggregation compared to the Cu—Cu. The increase in the free energy of Cu–Se interaction with respect to Cu–Cu interaction is not same with increasing temperature. The increase is 100% at 500 K and 143% at 1000 K. The increase in driving force for the Cu—Se aggregation is more at high temperatures.

The pair correlation, RDF, based excess entropy estimation for ionic melts and molecular liquids is shown to be accurate enough with less than 10% error.[41] RDF-based excess entropy calculations are also shown to be useful in understanding the disordered solids.[42] In this work, we have also computed the excess entropy for the Cu—Se and Cu—Cu system using the following equation, which is shown in Figure 9b.

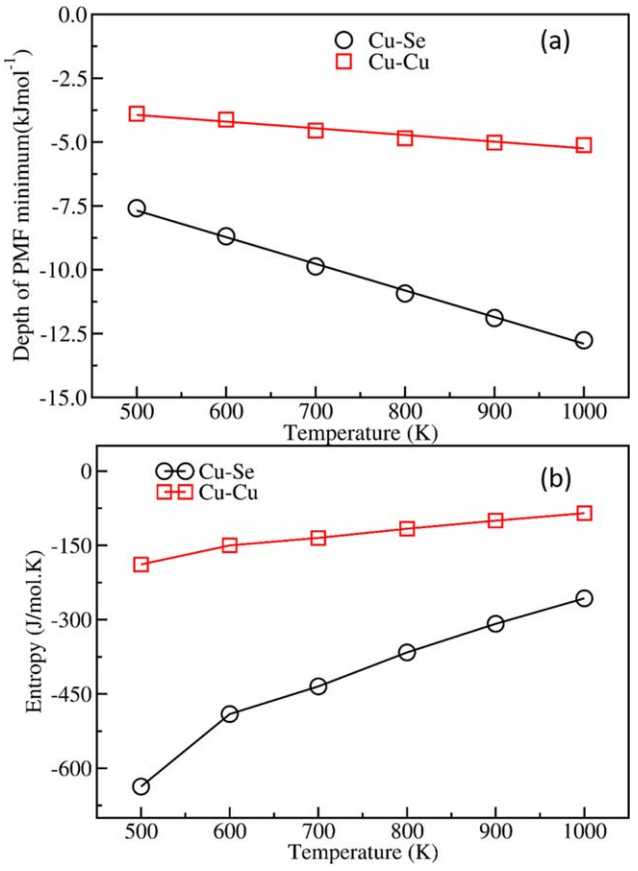

Figure 9. a) The free energy of aggregation for Cu—Cu and Cu—Se atoms is shown at different temperatures; solid line shows the straight line fit to the simulation data. b) The excess entropy associated with the Cu–Cu and Cu–Se interactions is presented at different temperatures. [Color figure can be viewed at wileyonlinelibrary.com]

$$S_{ex} = -2\pi\rho k_B \int [g(r)\ln g(r) - g(r) + 1] r^2 dr \quad (6)$$

The excess entropy is useful to understand the mechanism responsible for the change in the properties of the system. This excess entropy is found to be increasing for both the systems. The excess entropy change associated with the increase in temperature from 500 to 1000 K is 80 J/mol.K for Cu–Cu interactions and 387 J/mol.K for Cu–Se interactions. This shows that the Cu–Se interactions maximizes the entropy and minimizes the free energy (see Fig. 9a). From the above discussion, we may conclude that the Cu–Se interactions are more thermodynamically feasible than the Cu—Cu. Furthermore, it strongly suggests that increase in temperature may increase the probability for the Cu ions to diffuse into the Se layer by occupying the Se layer interstitial sites. This qualitative understanding is consistent with the experimentally reported structural analysis of the β-Cu_2Se.[10,11,20]

Conclusions

In this work, we have developed an empirical force-field for the β-Cu_2Se system, which is able to reproduce experimental structural, mechanical, and thermophysical properties of β-

Cu_2Se system. MD simulations are performed to study the structural evolution of the system with the temperature. Within the range of 500 to 1000 K, the average structure of the system is studied using the RDF calculations. RDF analysis shows, liquid like behavior of Cu ions and rigid motion for Se ions around their respective positions. The thermodynamics properties, PMF and excess entropy, are evaluated for the considered temperature range. The computed thermodynamic properties show that the Cu–Se interactions maximizes the entropy and minimizes the free energy. This shows that the Cu ions diffusion into the Se layer to occupy the interstitial positions is more thermodynamically favorable than aggregation with the other Cu ions.

Acknowledgments

The High Performance Computing (HPC) facility of Indian Institute of Technology Kanpur is gratefully acknowledged. SA would like to acknowledge the use of the computing facilities at Intra University Accelerator Centre in New Delhi, Institute of Mathematical Sciences in Chennai, CSIR-Fourth Paradigm Institute in Bengaluru and University of Hyderabad in Hyderabad. BG would like to thank Dr. Ajay Dhar for helpful discussions. SN would like to thank Dr. Shakti S Gupta for helpful discussions.

Keywords: Cu_2Se · density functional theory · force-field · molecular dynamics · thermoelectrics

How to cite this article: S. Namsani, B. Gahtori, S. Auluck, J. K. Singh. *J. Comput. Chem*. **2017**, *38*, 2161–2170. DOI: 10.1002/jcc.24865

[1] D. M. Rowe, In *Thermoelectrics Handbook*; CRC Press, **2005**; Chapter 58, p. 20.
[2] L. E. Bell, *Science* **2008**, *321*, 1457.
[3] G. S. Nolas, J. Poon, M. Kanatzidis, *MRS Bull.* **2006**, *31*, 199.
[4] W. Xie, X. Tang, Y. Yan, Q. Zhang, T. M. Tritt, *J. Appl. Phys.* **2009**, *105*, 113713.
[5] J. Li, Q. Tan, J.-F. Li, D.-W. Liu, F. Li, Z.-Y. Li, M. Zou, K. Wang, *Adv. Funct. Mater.* **2013**, *23*, 4317.
[6] E. S. Toberer, P. Rauwel, S. Gariel, J. Tafto, G. Jeffrey Snyder, *J. Mater. Chem.* **2010**, *20*, 9877.
[7] D.-Y. Chung, T. Hogan, P. Brazis, M. Rocci-Lane, C. Kannewurf, M. Bastea, C. Uher, M. G. Kanatzidis, *Science* **2000**, *287*, 1024.
[8] A. D. LaLonde, Y. Pei, G. Snyder, *J. Energy Environ. Sci.* **2011**, *4*, 2090.
[9] H. Wang, Y. Pei, A. D. LaLonde, G. J. Snyder, *Proc. Natl. Acad. Sci. USA* **2012**, *109*, 9705.
[10] H. Liu, X. Shi, F. Xu, L. Zhang, W. Zhang, L. Chen, Q. Li, C. Uher, T. Day, G. Snyder, *J. Nat. Mater.* **2012**, *11*, 422.
[11] B. Yu, W. Liu, S. Chen, H. Wang, H. Wang, G. Chen, Z. Ren, *Nano Energy* **2012**, *1*, 472.
[12] S. Kashida, J. Akai, *J. Phys. C Solid State* **1988**, *21*, 5329.
[13] R. M. Murray, R. D. Heyding, *Can. J. Chem.* **1975**, *53*, 878.
[14] R. D. Heyding, R. M. Murray, *Can. J. Chem.* **1976**, *54*, 841.
[15] Z. Vučić, O. Milat, V. Horvatić, Z. Ogorelec, *Phys. Rev. B* **1981**, *24*, 5398.
[16] M. C. Nguyen, J.-H. Choi, X. Zhao, C.-Z. Wang, Z. Zhang, K.-M. Ho, *Phys. Rev. Lett.* **2013**, *111*, 165502.
[17] K. Yamamoto, S. Kashida, *Solid State Ion.* **1991**, *48*, 241.
[18] M. Oliveria, R. K. McMullan, B. J. Wuensch, *Solid State Ion.* **1988**, *28–30*, 1332.
[19] H. Alam, S. Ramakrishna, *Nano Energy* **2013**, *2*, 190.
[20] H. Kim, S. Ballikaya, H. Chi, J.-P. Ahn, K. Ahn, C. Uher, M. Kaviany, *Acta Mater.* **2015**, *86*, 247.
[21] B. Qiu, X. Ruan, *Phys. Rev. B* **2009**, *80*, 165203.
[22] X. J. Tan, W. Liu, H. J. Liu, J. Shi, X. F. Tang, C. Uher, *Phys. Rev. B* **2012**, *85*, 205212.
[23] V. Varshney, S. S. Patnaik, C. Muratore, A. K. Roy, A. A. Voevodin, B. L. Farmer, *Comput. Mater. Sci.* **2010**, *48*, 101.
[24] J. D. Gale, *J. Chem. Soc., Faraday Trans.* **1997**, *93*, 629.
[25] J. D. Gale, A. L. Rohl, *Mol. Simul.* **2003**, *29*, 291.
[26] P. Blaha, K. Schwarz, G. K. H. Madsen, D. Kvasnicka, J. Luitz, *WIEN2k, An Augmented Plane Wave Plus Local Orbitals Program for Calculating Crystal Properties*; Vienna University of Technology: Austria, **2001**.
[27] J. P. Perdew, K. Burke, M. Ernzerhof, *Phys. Rev. Lett.* **1996**, *77*, 3865.
[28] S. J. Plimpton, *Comput. Phys.* **1995**, *117*, 1.
[29] S. Parker, G. Price, *Adv. Solid State Chem.* **1989**, *1*, 295.
[30] J. D. Gale, *J. Phys. Chem. B* **1998**, *102*, 5423.
[31] F. Birch, *Phys. Rev.* **1947**, *71*, 809.
[32] M. Råsander, L. Bergqvist, A. Delin, *J. Phys.: Condens. Matter* **2013**, *25*, 125503.
[33] M. Born, K. Huang, *Dynamical Theory of Crystal Lattices*; Clarendon Press: Oxford, **1998**.
[34] A. G. J. Beattie, *Appl. Phys.* **1969**, *40*, 4818.
[35] O. L. J. Anderson, *Phys. Chem. Solids* **1963**, *24*, 909.
[36] L. J. Walpole, *J. Phys. D: Appl. Phys.* **1986**, *19*, 457.
[37] D. A. McQuarrie, *Statistical Mechanics*; University Science Books: California, **2000**.
[38] Y. Tong, F. Yi, L. Liu, P. Zhai, Q. Zhang, *Comput. Mater. Sci.* **2010**, *48*, 343.
[39] E. Shoko, G. J. Kearley, V. K. Peterson, H. Mutka, M. M. Koza, J.-i. Yamaura, Z. Hiroi, G. J. Thorogood, *J. Phys.: Condens. Matter* **2014**, *26*, 305401.
[40] A. F. de Moura, K. Bernardino, C. J. Dalmaschio, E. R. Leite, N. A. Kotov, *Phys. Chem. Chem. Phys.* **2015**, *17*, 3820.
[41] R. Sharma, M. Agarwal, C. Chakravarty, *Mol. Phys.* **2008**, *106*, 1925.
[42] K. Binder, W. Kob, *Glassy Materials and Disordered Solids*; World Scientific Publishing Co, Pte. Ltd.: Singapore, **2005**.

Received: 23 March 2017
Revised: 24 May 2017
Accepted: 31 May 2017
Published online on 30 June 2017